doi.org/10.1002/cbdv.202200131

RESEARCH ARTICLE

CHEMISTRY & BIODIVERSITY

Cerium Oxide Nanoparticles Biosynthesized Using Fresh Green Walnut Shell in Microwave Environment and their Anticancer Effect on Breast Cancer Cells

Mine Sulak,[a] Gurbet Celik Turgut,[b] and Alaattin Sen*[c, d]

[a] Department of Mathematics and Science Education, Faculty of Education, University of Pamukkale, 20070, Denizli, Turkey

[b] Department of Organic Farming Business Management, Faculty of Applied Sciences, University of Pamukkale, 20600, Civril, Denizli, Turkey

[c] Department of Biology, Faculty of Arts & Sciences, University of Pamukkale, 20070, Denizli, Turkey, e-mail: sena@pau.edu.tr

[d] Department of Molecular Biology and Genetics, Faculty of Life and Natural Sciences, University of Abdullah Gul, 38080, Kayseri Turkey, e-mail: sena@agu.edu.tr

In this study, cerium oxide nanoparticles (CONPs) were synthesized using fresh green walnut shell extract in microwave environment. The morphology and structure of the CONPs were determined using ultraviolet-visible (UV/VIS), attenuated total reflection-Fourier transform infrared (ATR-FT-IR), X-ray diffraction (XRD), energy-dispersive X-ray (EDX) spectroscopy, and scanning electron microscopy (SEM). Crystal purple staining, Annexin V-FITC detection, RT-PCR, P53, and NF-κB luciferase reporter assays were performed to evaluate the mechanism of action of CONPs in breast cancer cell lines (MCF7). The biosynthesized CONPs showed cytotoxic effects and induced apoptosis in MCF7 cells. Furthermore, CONPs induced P53 expression and suppressed NF-κB gene expression, both of which were confirmed using reporter assays. Based on the present results, it was concluded that CONPs can induce apoptosis by acting on P53 at the transcriptional level and may cause cell death by suppressing NF-κB-mediated transcription.

Keywords: cerium oxide nanoparticles, breast cancer, P53, NF-κB, apoptosis.

Introduction

Despite multimodal treatment approaches, such as surgery, radiation, and chemotherapy, breast cancer continues to be a global concern owing to its increasing prevalence and mortality rate.[1] The therapeutic potential of chemotherapeutic drugs is limited due to non-specific cytotoxicity to cancer cells and poor selectivity in drug delivery. Nanoparticles (NPs) can boost therapeutic efficacy by directly and selectively targeting cancerous cells. NP-based therapy has therefore emerged as an attractive alternative to traditional chemotherapeutics for the effective treatment of breast cancer.[2,3]

Metal oxides with different physical and chemical properties based on their band gaps are important materials for many applications in science and technology. The metal oxide form of cerium, one of the most reactive rare-earth elements, is preferred in various fields owing to its wide band gap, high dielectric constant, non-toxicity, economic applicability, and long-term stability Cerium oxide nanoparticles (CONPs) exhibit antibacterial, anticancer, anti-inflammatory, anti-Alzheimer, and antioxidant activities as well as the ability to absorb UV light.[4–9]

Various techniques have been employed for synthesizing metal oxide NPs, including environment-friendly green synthesis,[10] sol-gel, inert gas condensation,[11] mechanical etching,[12] and ultrasonic spray pyrolysis.[13] Environmental pollution caused by other methods, however, emphasizes the importance of green synthesis. Furthermore, green synthesis is cost-effective, the plants used for synthesis are diverse, and the metal scale used is broad.[14]

The green synthesis involves plants and plant extracts, microorganisms, fungi, proteins, amino acids, vitamins, and polysaccharides.[15] One of the most significant shortcomings of the biosynthesis method is its slow reaction rate, an issue that can be addressed by employing microwave (MW) to synthesize NPs. MWs are a form of electromagnetic energy with frequencies ranging from 300 MHz to 300 GHz. MW rapid heating is used to synthesize metallic nanostructures in a solution. Various experimental parameters can be altered to control the morphology and dimensions of the nanostructure (such as the metallic salt and surfactant polymer concentration, solvent, and reaction temperature). The reaction is faster, the required reaction temperature is reached faster, nanocomposites are smaller in size, size distribution is narrower, and the degree of crystallization is higher with the MW technique, compared to the traditional oil bath heating method.

In this study, CONPs were obtained from fresh green walnut shell extracts using the MW heating method. The characteristic structure, particle distribution, and size of the obtained CONPs were determined using X-ray diffraction (XRD), ultraviolet-visible (UV/VIS) spectroscopy, scanning electron microscopy (SEM), and energy-dispersive X-ray (EDX) spectroscopy. The structures formed after the reaction and absorbed on the NP surface were examined using attenuated total reflection-Fourier transform infrared (ATR-FT-IR) spectroscopy. To determine the potential biological effects of the CONPs, the crystal violet method was used to determine the 50% inhibitory concentration (IC_{50}) in a breast cancer cell lines (MCF7). This dose was used in subsequent studies.

Results and Discussion

Breast cancer is a significant concern due to its increasing prevalence and mortality rates worldwide. Since the current drugs used in cancer treatment are delivered non-specifically, they cause severe damage to normal cells. As a result, they have limited selectivity. NPs have recently attracted the attention of scientists and pharmaceutical companies due to their ability to increase therapeutic efficacy by directly and selectively targeting cancerous cells. The goal of this study was to determine the possible therapeutic effect of CONPs on breast cancer.

In chemical synthesis, metal ions are compressed with a chemical reducing agent, forming a metal core to produce metal oxide NPs. Particles are controlled by a capping agent that prevents them from aggregating. However, in biological synthesis, primary plant compounds such as flavonoids, phenolic compounds, terpenoids, heterocyclic compounds, enzymes, peptides, polysaccharides, saponins, and tannins provide the reducing and capping agents. The transformation of the initial green solution into brown due to MW-assisted synthesis of CONPs from fresh green walnut shell extract and $CeCl_3 \cdot 7H_2O$ solution in a basic environment is the first evidence of the formation of CONPs (*Scheme 1*).

MW-assisted synthesis is a simple and effective method for the rapid and abundant production of metallic oxide nanoparticles. The MW rapid heating method has been applied in the synthesis of metallic oxide nanostructures in solution. Along with spherical nanoparticles, materials such as single-crystalline polygonal sheets, rods, wires, and tubes can also be prepared in a few minutes using MW heating. The morphology and dimensions of the nanostructure can be controlled by varying certain experimental parameters (such as metallic salt, time, solvent, and reaction temperature). Compared to the traditional oil bath heating method, nanocomposites prepared via the MW method are smaller, have a narrower size distribution, and have a higher degree of crystallization.

Following the synthesis, the CONPs were characterized using UV/VIS spectroscopy, a fast and straightforward method for the characterization of biosynthetic CONPs.[16] The UV/VIS spectra of CONPs obtained by using walnut shell extract and cerium(III) chloride heptahydrate are shown in *Figure 1*. The

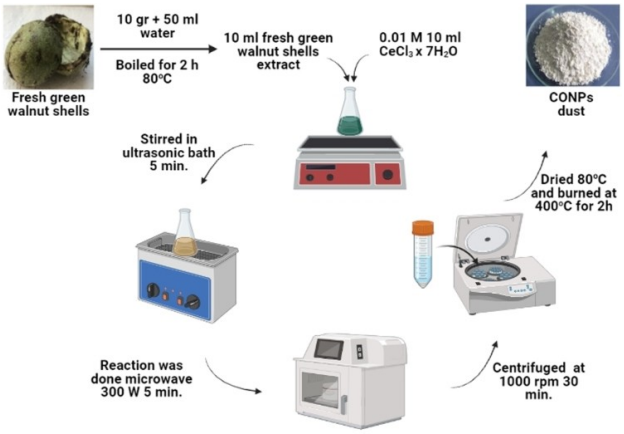

Scheme 1. Synthesis scheme of CONPs obtained using fresh green walnut shell extract. This figure was made using the BioRender program (https://biorender.com/).

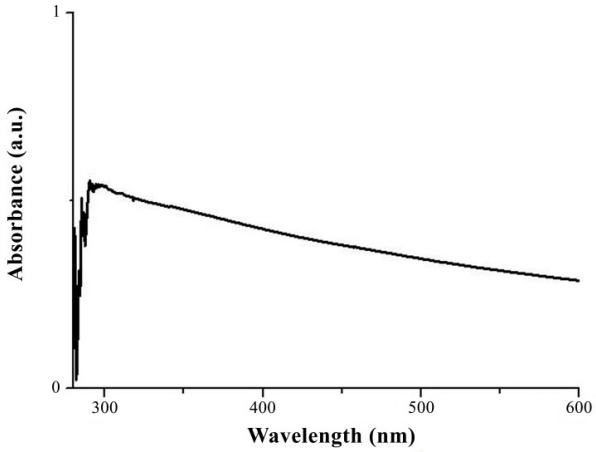

Figure 1. UV/VIS image of CONPs

absorption peak of the CONPs at 298 nm is consistent with previous studies.[17–20]

The FT-IR spectrum (*Figure 2*) of the CONPs was used to determine the compound's chemical structures and functional groups. The solid and wide absorption peak in the frequency range 3000 to 3750 cm^{-1} corresponds to the O–H and N–H stretching from carbohydrates, polyphenols, and proteins in plants. Absorption peaks around 1571 cm^{-1} indicate weak C–H stretching of alkane compounds. The vibrational band of the ether functional group (C–O–C) found in polysaccharides was observed at 1076 cm^{-1}. The Ce–O stretching band is the most significant proof of the formation of CONPs, which are synthesized by the effective interaction of the bioorganic components of the walnut shell extract with Ce_3^+.[21,22]

The surface of cerium(IV) oxide was examined morphologically using the SEM image of nano-sized cerium(IV) oxide obtained from cerium(III) chloride heptahydrate by green synthesis (*Figure 3*). As a result of the examination, it was determined that the particles were dispersed in a spherical and homogeneous manner at the nanoscale. The particle sizes were on average 22–28 nm.

The EDX spectrum of CONPs is given in *Figure 3C*. It is seen that the cerium in the structure of the prepared CONPs contains 42.05% Ce and 57.95% O. It can also be seen that the results of the EDX analysis are consistent with the results of the SEM and XRD analyses. A similar outcome has been reported for CONPs prepared with *Moringa oleifera* extract.[23]

In *Figure 4*, the XRD (powder) method was used to determine the crystal formation of cerium(IV) oxide prepared by the MW-assisted green synthesis method.

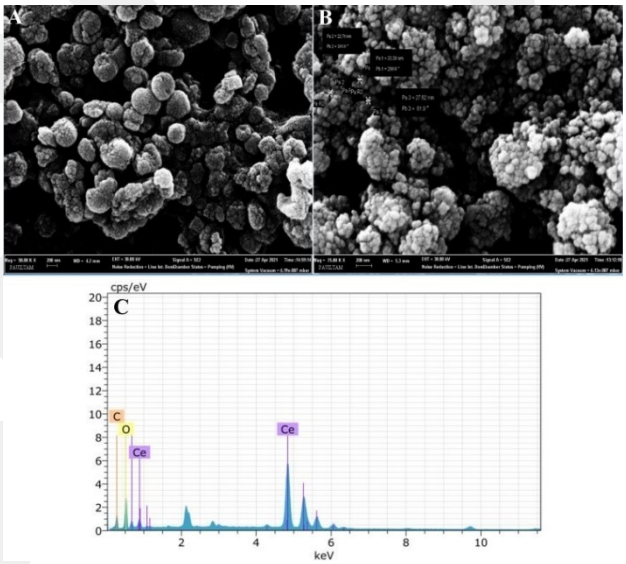

Figure 3. SEM images of CONPs **A**) at 50.00 kx magnification, **B**) at 75.00 kx magnification. **C**) EDX spectrum of CONPs.

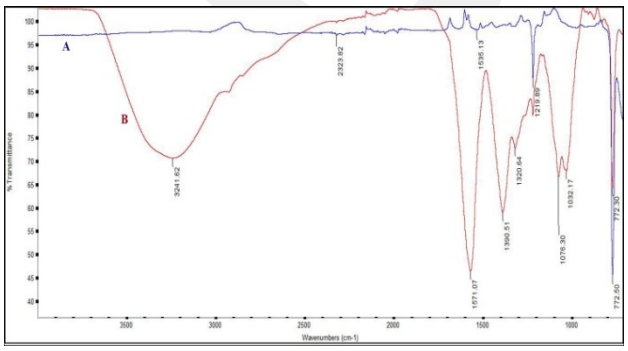

Figure 2. ATR-FT-IR spectra of **A**) CONPs obtained from fresh green walnut shell extract. **B**) Fresh green walnut shell extract.

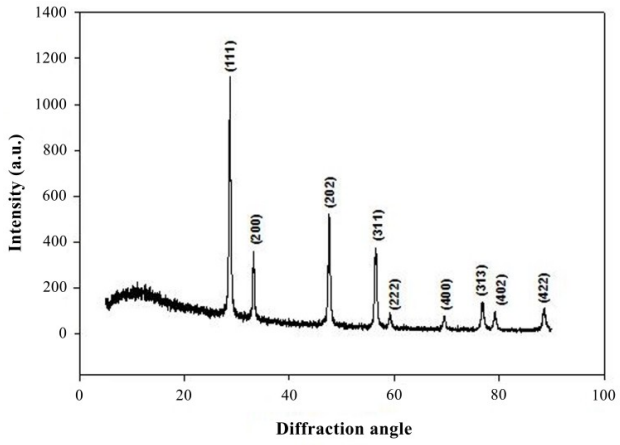

Figure 4. X-Ray Diffractogram/Diffraction Patterns of CONPs.

The 2θ characteristic reflection peaks of nano-cerium(IV) oxide are respectively 23.64°, 28.25°, 42.70°, 51.54°, 54.19°, 64.54°, 71.79°, 74.31°, and 83.66° and the index values are (111), (200), (202), (311), (222), (400), (313), (402), and (422). The indices of these peaks agree with JCPDS File Card No. 96-900-9009 and correspond to the cubic structure of CONPs. The average crystallite size of CONPs obtained using fresh green walnut shell extract is calculated by Scherrer's formula.[24] Using Equation 1, the crystallite size was calculated for the peaks (002) and (111), and the values were found to be ≈19.2 nm. The obtained values are compatible with the literature.[25] Furthermore, XRD analysis demonstrated the absence of impurities in the CONPs prepared and confirmed the particle size determined by SEM.

Debye Scherrer equation:

$$D = K\lambda/\beta\cos\theta \quad (1)$$

where D: Average crystallite size, K: a constant equal to 0.94, λ: the wavelength of X-ray radiation (0.154 nm), β: the slit apex width of the crown (in radians) and 2θ: corresponds to Bragg's angle (degrees).

After completing the synthesis and characterization procedures, the CONPs were tested for their potential anticancer activity in breast cancer cells to identify more targeted therapeutic candidates. To accomplish this, the crystal violet staining method was used to determine the IC_{50} value of the CONPs in MCF7 cells. As shown in *Figure 5*, the CONPs showed a dose-dependent cytotoxic effect on MCF7 cells. The IC_{50} value of CONPs was 134.28 μg/mL. A study conducted on the MCF7 cell lines with CONPs was reported, which was compatible with our findings.[26] Furthermore, research has revealed that CONPs exhibit varying degrees of cytotoxicity in different cancer cell lines.[26–28]

Following the determination of the IC_{50} value of CONPs, the apoptotic effect of CONPs was investigated using Annexin V assay to justify the mechanistic basis of their cytotoxic effect in breast cancer cells. After administration of the IC_{50} dose of CONPs, the rates of viable, dead, and apoptotic cells were determined using Arthur image-based cytometer. As seen in *Figure 6*, the rate of apoptotic, live, and dead MCF7 cells after treatment of CONPs was found to be 16%, 78%, and 5%, respectively. This finding demonstrated that CONPs induced apoptosis in breast cancer cells. In the literature, it is found that CONPs cause apoptosis in various cancer cell lines, which is similar to our findings.[29–31]

However, these results do not indicate exactly which pathway is responsible for inducing apoptosis. Knowing cell death mechanisms in cancer treatments is critical for drug-targeted therapeutical strategies. For this purpose, the effect of CONPs on the expression of P53 and NF-κB genes, which are essential in initiating the apoptotic cascade, was studied at the transcriptional level.

The effects of CONPs on P53 and NF-κB mRNA expression in MCF7 cells were analyzed using qRT-PCR, and the results are shown in *Figure 7*. The mRNA expression level of P53 increased 2.46-fold, while the expression level of NF-κB mRNA decreased 9.25-fold after treatment with CONPs. It was reported that CONPs induce increased P53 expression in lung cells and colorectal carcinoma cells.[31,32]

In addition to determining the effect of CONPs on P53 and NF-κB mRNA expression levels, the binding of CONPs to P53 and NF-κB response elements was experimentally validated. It was found that CONPs increased the P53-response element (RE) activity al-

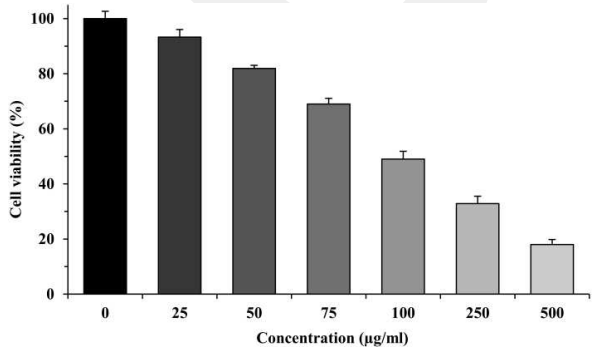

Figure 5. Cytotoxicity of CONPs against MCF7 cells. Results are mean ± SEM values for three independent experiments.

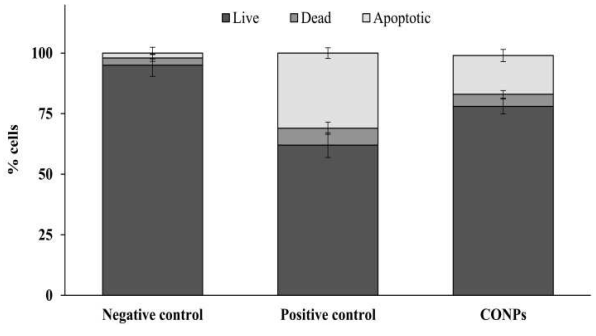

Figure 6. Apoptosis assay in MCF7 cells after CONPs treatment. H_2O_2 was used as a positive control for cells. Data are representative of at least three independent experiments.

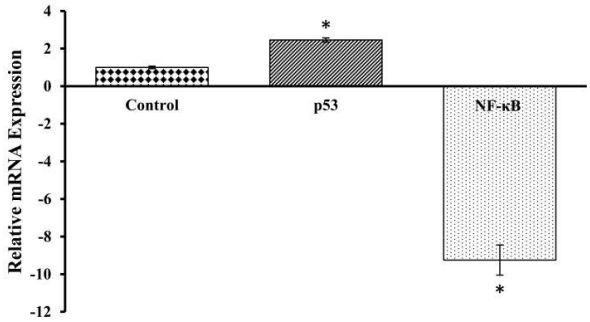

Figure 7. Effects of CONPs treatment on P53 and NF-κB mRNA expression in MCF7 cells. β-actin has been used as a housekeeping gene. * Indicates significantly different at $P < 0.05$.

most as much as doxorubicin in the P53-RE luciferase constructs (*Figure 8A*). It was also confirmed that CONPs reduced NF-κB-RE activity in LPS-induced cells harboring the NF-κB-RE luciferase construct (*Figure 8B*). Similar repression was reported earlier, wherein CONPs inhibited LPS-induced MAP kinase/NF-kB-mediated severe sepsis.[33] As a result, P53 induction and suppression of NF-κB-driven transcription are two

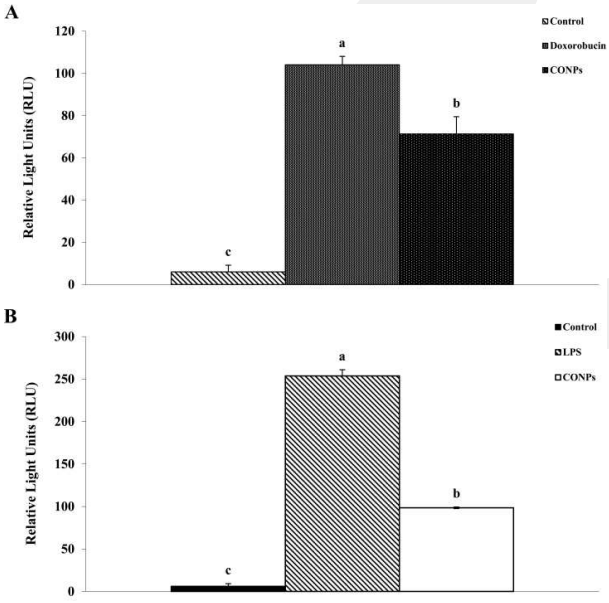

Figure 8. A) Cells, transfected with P53 firefly luciferase construct, were treated with doxorubicin (control) and CONPs, and luciferase activities were measured. **B**) Cells transfected with the NF-κB firefly luciferase construct were stimulated with LPS, then treated with CONPs, and their luciferase activities were measured. P53 and NF-κB dependent promoter activities are presented in relative light unit (RLU). Results are expressed as relative mean ± standard error and presented as the mean from three independent experiments. At $P < 0.05$, means with different letters in the same column are substantially different.

significant mechanisms behind the apoptotic activity of CONPs, as demonstrated by the findings.

Conclusions

As an alternative to chemical synthesis, CONPs were synthesized biologically using fresh green walnut shell extract, which has not been previously reported, without any additional reducing and capping agents. All physical and chemical analyses confirmed the synthesis of CONPs with a face-centered cubic phase and an average size of 26 ± 2 nm. CONPs induced P53 gene expression at the transcriptional level and suppressed NF-κB-mediated transcription, resulting in cytotoxic and apoptotic effects in MCF7 cells. Nevertheless, cell death cascades need to be investigated in more detail.

Experimental Section

Plant Materials and Preparation

Fresh green walnuts were purchased from Çivril/Denizli local market in late September 2020 and stored at −80 °C until extracted. After peeling fresh green walnuts, the shells were processed in a food processor and cut into small pieces. Fresh green walnut shells (10 g) and deionized water (50 mL) were added to an Erlenmeyer flask and heated on a magnetic heater at 80 °C for 2 h. Walnut shell extracts were obtained by filtering the resulting mixture through Whatman filter paper (Grade GF/B: 1.0 μm) and were freshly prepared to synthesize CONPs.

MW-Assisted Green Synthesis of CONPs

As cerium(III) chloride heptahydrate ($CeCl_3 \cdot 7H_2O$) and sodium hydroxide (NaOH) obtained from Sigma–Aldrich, Inc. (St. Louis, MO, USA) were of analytical purity, they were used without any purification. 10 mL of 0.01 M $CeCl_3 \cdot 7H_2O$ and 10 mL of fresh walnut shell extract were combined in a beaker, adjusted to pH 10 using NaOH, and homogenized in an ultrasonic bath for 5 min. The solution was completed within 5 min using a household MW oven (LG, MH-4048GW) at 300 W. The solution was then cooled to room temperature. The resulting brown suspension was centrifuged at 10000 rpm for 30 min, washed with ethanol, and centrifuged again. The final residue collected at the bottom was oven dried at 80 °C. It was then calcined at 400 °C for 2 h to remove any impurities. After

calcination, the sample was crushed in a mortar and ground into powder.

Characterization of CONPs

Preliminary characterization of CONPs was performed using UV/VIS spectroscopy. The powdered CONPs were suspended in double-distilled water (50 mg/mL) and then left in an ultrasonic bath for 10 min to make a homogeneous suspension. CONPs were analyzed spectrophotometrically in quartz cuvettes with an optical path length of 1 mm, in the wavelength range of 200–400 nm, with water as the reference solution (UV/VIS-1601, Shimadzu, Kanagawa, Japan).

ATR-FT-IR measurements of the synthesized CONPs were made with 4 cm^{-1} resolution and 50 scans (PerkinElmer Inc., Norwalk, CT, USA).

To determine the crystal phases in the structure of CONPs obtained from the fresh green walnut extract and to investigate the crystal sizes, CuK_α radiation (λ as 1.54060 Å), in the range of 5° to 90° to 80 XRD APD 2000 PRO (GNR, Novara, Italy), was used. The XRD spectra were compared with the JCPDS (Joint Committee on Powder Diffraction Standards) XRD data analysis card. The average dimensions of CONPs were calculated according to the Debye Scherrer equation.[34]

SEM was used to determine the surface properties of CONPs. The surface morphologies of the prepared NPs were determined using an electron microscope (Zeiss Supra 40 VP, Oberkochen, Germany) with a resolution of 1.2 nm. EDX analyses were carried out to perform elemental analysis of the CONPs obtained by the green synthesis method (Quorum Q150R ES, Quorum Technologies Ltd., UK).

Cell Culture

The human breast adenocarcinoma cell lines MCF7 was grown in Dulbecco's Modified Eagle Medium, supplemented with 10% heat-inactivated fetal bovine serum and 1% antibiotic in a humidified atmosphere of 95% air with 5% CO_2, at 37 °C, and was subcultured twice a week.

Cell Viability Assay

MCF7 cells were seeded into 96-well plates at a density of 2000 cells/well after trypsinization. Following 24 h attachment, the cells were treated with different concentrations of CONPs. As a control, cells not incubated with CONPs were treated similarly. After 24 h incubation, the medium was drained, and 0.5% crystal violet (w/v, in 50% methanol) was added to each well. Cells were incubated at room temperature for 10 min and then washed with water. Then, the adsorbed dye was eluted with Na-citrate (0.1 M Na-citrate in 50% ethanol, pH 4.2). The absorbance proportional to cell viability was measured using a spectrophotometer (Thermo Scientific Multiskan GO Microplate Spectrophotometer) at 600 nm wavelength. Cell viability was monitored as a percentage of viable cells compared to control, untreated cells.[35]

Apoptosis

To assess the apoptotic effects of CONPs, MCF7 cells were incubated overnight after seeding at 2×10^5 cells/well in 6-well plates. Following incubation, the cells were treated with CONPs at IC_{50} for 24 h; hydrogen peroxide (H_2O_2) was used as a positive control.[36] The apoptotic assay was performed with a novel fluorescent cell counter (Arthur-NanoEntek) using the Annexin V-FITC Apoptosis Detection Kit (BioVision).

RNA Isolation and RT-PCR

Total RNA from control and treated cells was isolated via RNeasy Plus Universal Mini Kit (Qiagen) according to the manufacturer's instructions. RNA concentration and purity were determined at 260/280 nm using NanoDrop 1000 spectrophotometer (MaestroNano Micro-volume Spectrophotometer, USA). Total RNA was reverse-transcribed using Easy Script cDNA Synthesis Kit (ABM) according to the manufacturer's instructions. RT-PCR assay was carried out using gene-specific primers. β-actin was used as the housekeeping gene to normalize expression levels. RT-PCR assay was performed with Exicycler 96 Thermal Block (Bioneer, Korea) using KiloGreen 2X qPCR Master Mix (ABM, Canada). Values of cycle threshold (Ct) obtained in quantification were used to calculate fold changes in mRNA abundance according to the $2^{-\Delta\Delta Ct}$ method.[37]

Luciferase Reporter Assay

To determine the effect of CONPs on transcriptional activity of NF-κB and P53, pGL4.32 [luc2P/NF-κB/Hygro] and pGL4.38 [luc2P/p53 RE/Hygro] plasmids containing the Renilla gene for luciferase normal-

ization were transfected separately into MCF7 cells using Fugene HD transfection reagent (Promega).[37]

To evaluate NF-κB transcriptional activity, cells were stimulated with 2 μg/mL lipopolysaccharide (LPS) after 24 h of transfection and then incubated with CONPs at IC_{50} for 6 h after stimulation. Similarly, to assess P53 transcriptional activity, cells were treated with the CONPs at IC_{50} after 24 h of transfection. Doxorubicin was used as a positive control. After 24 h incubation with CONPs, luciferase activities were measured using the Dual-Glo Luciferase assay kit (E2920, Promega) and the Synergy HTX luminometer (BioTek).

Statistical Analysis

Statistical analysis was performed using Minitab 13 statistical software package. All results were expressed as mean ± Standard Error of Means (SEMs). Comparison between groups was assessed using Student's *t*-test, and $P < 0.05$ was determined as the level required for statistical significance.

Data Availability Statement

The data that support the findings of this study are available from the corresponding author upon reasonable request.

Author Contribution Statement

M. S. and G. C. T. performed the experiments, analyzed the data and wrote the article. A. S. and M. S. contributed to the samples/reagents/materials/analysis tools and analyzed the data. M. S., G. C. T. and A. S. conceived and designed the experiments.

References

[1] H. Sung, J. Ferlay, R. L. Siegel, M. Laversanne, I. Soerjomataram, A. Jemal, F. Bray, 'Global Cancer Statistics 2020: GLOBOCAN Estimates of Incidence and Mortality Worldwide for 36 Cancers in 185 Countries', *Ca-Cancer J. Clin.* **2021**, *71*, 209–249.

[2] X. Fang, J. Cao, A. Shen, 'Advances in anti-breast cancer drugs and the application of nano-drug delivery systems in breast cancer therapy', *J. Drug Delivery Sci. Technol.* **2020**, *57*, 101662.

[3] J. Panda, B. S. Satapathy, S. Majumder, R. Sarkar, B. Mukherjee, B. Tudu, 'Engineered polymeric iron oxide nanoparticles as potential drug carrier for targeted delivery of docetaxel to breast cancer cells', *J. Magn. Magn. Mater.* **2019**, *485*, 165–173.

[4] Y. Gao, K. Chen, J. L. Ma, F. Gao, 'Cerium oxide nanoparticles in cancer', *OncoTargets Ther.* **2014**, *7*, 835–840.

[5] D. Girija, H. S. B. Naik, C. N. Sudhamani, B. V. Kumar, 'Cerium oxide nanoparticles-a green, reusable, and highly efficient heterogeneous catalyst for the synthesis of polyhydroquinolines under solvent-free conditions', *Arch. Appl. Sci. Res.* **2011**, *3*, 373–382.

[6] M. Zhang, C. Zhang, X. Zhai, F. Luo, Y. Du, C. Yan, 'Antibacterial mechanism and activity of cerium oxide nanoparticles', *Sci. China Mater.* **2019**, *62*, 1727–1739.

[7] P. Eriksson, A. A. Tal, A. Skallberg, C. Brommesson, Z. Hu, R. D. Boyd, W. Olovsson, N. Fairley, I. A. Abrikosov, X. Zhang, K. Uvdal, 'Cerium oxide nanoparticles with antioxidant capabilities and gadolinium integration for MRI contrast enhancement', *Sci. Rep.* **2018**, *8*, 1–12.

[8] S. M. Hirst, A. S. Karakoti, R. D. Tyler, N. Sriranganathan, S. Seal, C. M. Reilly, 'Anti-inflammatory properties of cerium oxide nanoparticles', *Small* **2009**, *5*, 2848–2856.

[9] D. Barbara, S. Sandro, B. Elisabetta, D. L. Silvia, A. R. Phani, F. Stefano, A. Fernanda, C. P. Maria, C. Annamaria, 'Cerium Oxide Nanoparticles Trigger Neuronal Survival in a Human Alzheimer Disease Model By Modulating BDNF Pathway', *Curr. Nanosci.* **2009**, *5*, 167–176.

[10] Z. H. Wang, C. J. Choi, B. K. Kim, J. C. Kim, Z. D. Zhang, 'Magnetic Fe-Co and Its Oxide Nanopowders Produced by Chemical Vapor Condensation', *Mater. Trans.* **2005**, *46*, 2052–2056.

[11] C. Suryanarayana, B. Prabhu, 'Synthesis of nanostructured materials by inert-gas condensation methods', *Nanostruct. Mater.* **2007**, 47–90.

[12] L. C. Damonte, L. M. Zélis, B. M. Soucase, M. H. Fenollosa, 'Nanoparticles of ZnO obtained by mechanical milling', *Powder Technol.* **2004**, *148*, 15–19.

[13] S. C. Tsai, Y. L. Song, C. S. Tsai, C. C. Yang, W. Y. Chiu, H. M. Lin, 'Ultrasonic spray pyrolysis for nanoparticles synthesis', *J. Mater. Sci.* **2004**, *39*, 3647–3657.

[14] S. Iravani, 'Green synthesis of metal nanoparticles using plants', *Green Chem.* **2011**, *13*, 2638–2650.

[15] X. Zhu, K. Pathakoti, H. M. Hwang, 'Green synthesis of titanium dioxide and zinc oxide nanoparticles and their usage for antimicrobial applications and environmental remediation', *Green Synth., Charact. and Appl. of Nanopart.* **2019**, 223–263.

[16] D. Philip, 'Synthesis and Spectroscopic Characterization of Gold Nanoparticles', *Spectrochim. Acta Part A* **2008**, *71*, 80–85.

[17] B. Anand, A. Muthuvel, V. Mohana, S. Anandhi, M. Pavithra, 'Effect of chemically synthesis compared to biosynthesized CeO2 NPS using aqueous extract of Momordica Charantia', *Int. J. Res. Appl. Sci. Eng. Technol.* **2018**, *6*, 1073–1079.

[18] I. Nurhasanah, W. Saftri, Z. Arifn, A. Subagio, T. Windarti, 'Antioxidant activity and dose enhancement factor of CeO2 nanoparticles synthesized by precipitation method', *Iop. Conf. Ser. Mater. Sci. Eng.* **2018**, *432*, 012031.

[19] A. Arumugam, C. Karthikeyan, A. S. H. Hameed, K. Gopinath, S. Gowri, V. Karthika, 'Synthesis of cerium oxide nanoparticles using Gloriosa superba L. leaf extract and

their structural, optical and antibacterial properties', *Mater. Sci. Eng.* **2015**, *49*, 408–415.
[20] M. M. Ali, H. S. Mahdi, A. Parveen, A. Azam, 'Optical Properties of cerium oxide (CeO2) nanoparticles synthesized by hydroxide mediated method', *AIP Conf. Proc.* **2018**, *1953*, 030044.
[21] G. J. Brewer, P. J. Price, 'Viable cultured neurons in ambient carbon dioxide and hibernation storage for a month', *NeuroReport* **1996**, *7*, 1509–1512.
[22] E. K. Goharshadi, S. Samiee, P. Nancarrow, 'Fabrication of cerium oxide nanoparticles: characterization and optical properties', *J. Colloid Interface Sci.* **2011**, *356*, 473–480.
[23] S. A. Mahmud, 'Biosynthesis of CeO2 NPs using the optimal extract of *Moringa olifera*', *Int. J. Res. Appl. Sci. Eng. Technol.* **2016**, *10*, 37–39.
[24] M. Sharma, S. Murugavel, D. K. Shukla, F. M. De Groot, 'Reversal in the lattice contraction of α-Fe_2O_3 nanoparticles', *J. Phys. Chem. C* **2018**, *122*, 9292–9301.
[25] M. Darroudi, S. Javad, R. Kazemi, H. Ali, 'Food-directed synthesis of cerium oxide nanoparticles and their neurotoxicity effects', *Ceram. Int.* **2014**, *40*, 7425–7430.
[26] A. A. A. Al-Ali, R. K. Jawad, 'Cerium Oxide Nanoparticles Ceo2np and Retinoic Acid Trigger Cytotoxicity and Apoptosis Pathway in Human Breast Cell Lines', *Annals of R. S. C.B* **2021**, *25*, 8448–8477.
[27] L. D. Marzi, A. Monaco, J. D. Lapuente, D. Ramos, M. Borras, M. D. Gioacchino, S. Santucci, A. Poma, 'Cytotoxicity and genotoxicity of ceria nanoparticles on different cell lines *in vitro*', *Int. J. Mol. Sci.* **2013**, *14*, 3065–3077.
[28] G. Renu, V. V. D. Rani, S. V. Nair, K. R. V. Subramanian, V. K. Lakshmanan, 'Development of Cerium Oxide Nanoparticles and Its Cytotoxicity in Prostate Cancer Cells', *Adv. Sci. Lett.* **2012**, *5*, 1–9.
[29] E. Nourmohammadi, H. Khoshdel-Sarkarizi, R. Nedaeinia, H. R. Sadeghnia, L. Hasanzadeh, M. Darroudi, R. K. Oskuee, 'Evaluation of anticancer effects of cerium oxide nanoparticles on mouse fibrosarcoma cell lines', *J. Cell. Physiol.* **2019**, *234*, 4987–4996.
[30] S. Hussain, F. Al-Nsour, A. B. Rice, J. Marshburn, B. Yingling, Z. Ji, J. I. Zink, N. J. Walker, S. Garantziotis, 'Cerium dioxide nanoparticles induce apoptosis and autophagy in human peripheral blood monocytes', *ACS Nano* **2012**, *6*, 5820–5829.
[31] S. Mittal, A. K. Pandey, 'Cerium oxide nanoparticles induced toxicity in human lung cells: role of ROS mediated DNA damage and apoptosis', *BioMed Res. Int.* **2014**, 891934.
[32] A. Datta, S. Mishra, K. Manna, K. D. Saha, S. Mukherjee, S. Roy, 'Pro-Oxidant Therapeutic Activities of Cerium Oxide Nanoparticles in Colorectal Carcinoma Cells', *ACS Omega* **2020**, *5*, 9714–9723.
[33] V. Selvaraj, N. Nepal, S. Rogers, N. D. P. K. Manne, R. Arvapalli, K. M. Rice, S. Asano, E. Fankenhanel, J. Y. Ma, T. Shokuhfar, M. Maheshwari, E. R. Blougha, 'Cerium oxide nanoparticles inhibit lipopolysaccharide induced MAP kinase/NF-κB mediated severe sepsis', *Data Brief* **2015**, *4*, 105–115.
[34] R. Pielaszek, 'FW15/45M method for determination of the grain size distribution from powder diffraction line profile', *J. Alloys Compd.* **2004**, *382*, 128–132.
[35] G. Celik, H. Akca, A. Sen, 'Investigation of aromotase inhibition by several dietary vegetables in human non-small cell lung cancer cell lines', *Turk Biol. Derg.* **2013**, *38*, 207–217.
[36] C. Sahin, D. Mutlu, F. Nasirli, G. Mahmoudi, F. I. Zubkov, S. Arslan, N. M. Dogan, 'New iridium bis-terpyridine complexes: synthesis, characterization, antibiofilm and anticancer potentials', *BioMetals* **2021**, *34*, 701–713.
[37] G. C. Turgut, D. Doyduk, Y. Yıldırır, S. Yavuz, A. Akdemir, A. Dişli, A. Sen, 'Computer design, synthesis, and bioactivity analyses of drugs like fingolimod used in the treatment of multiple sclerosis', *Bioorg. Med. Chem.* **2017**, *25*, 483–495.

Received February 11, 2022
Accepted June 29, 2022

